ACS APPLIED MATERIALS & INTERFACES

Research Article

www.acsami.org

Quasi-in-Situ Single-Grain Photoelectron Microspectroscopy of Co/PPy Nanocomposites under Oxygen Reduction Reaction

Patrizia Bocchetta,[†] Matteo Amati,[‡] Benedetto Bozzini,*[,†] Massimo Catalano,[§] Alessandra Gianoncelli,[‡] Luca Gregoratti,[‡] Antonietta Taurino,[§] and Maya Kiskinova[‡]

[†]Dipartimento di Ingegneria dell'Innovazione, Università del Salento, via Monteroni, 73100 Lecce, Italy

[‡]Elettra-Sincrotrone Trieste S.C.p.A., Strada Statale 14, km 163.5 in Area Science Park, 34012 Basovizza, Trieste, Italy

[§]Institute for Microelectronics and Microsystems, IMM-CNR, via Monteroni, 73100 Lecce, Italy

Supporting Information

ABSTRACT: This paper reports an investigation into the aging of pyrolyzed cobalt/polypyrrole (Co/PPy) oxygen reduction reaction (ORR) electrocatalysts, based on quasi-in-situ photoelectron microspectroscopy. The catalyst precursor was prepared by potentiostatic reverse-pulse coelectrodeposition from an acetonitrile solution on graphite. Accelerated aging was obtained by quasi-in-situ voltammetric cycling in an acidic electrolyte. Using photoelectron imaging and microspectroscopy of single Co/PPy grains at a resolution of 100 nm, we tracked the ORR-induced changes in the morphology and chemical state of the pristine material, consisting of uniformly distributed ~20 nm nanoparticles, initially consisting of a mixture of Co(II) and Co(III) oxidation states in almost equal amounts. The evolution of the Co 2p, O 1s, and N 1s spectra revealed that the main effects of aging are a gradual loss of the Co present at the surface and the reduction of Co(III) to Co(II), accompanied by the emergence and growth of a N 1s signal, corresponding to electrocatalytically active C−N sites.

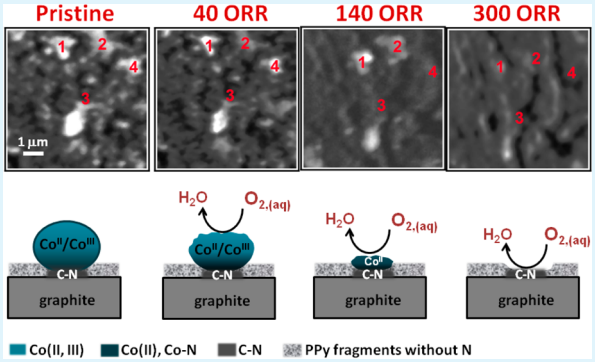

KEYWORDS: *cobalt, polypyrrole, oxygen reduction, electrocatalyst, nanocomposites, photoelectron microscopy, X-ray photoelectron spectroscopy*

1. INTRODUCTION

Nonprecious metal−nitrogen−carbon (M/N/C) catalysts have been extensively studied as possible substitutes of Pt-based materials for air cathodes, since the discovery of the electrochemical activity of cobalt phthalocyanine and of transition metal macrocycles, in general, toward the oxygen reduction reaction (ORR).[1] Intense research activities were dedicated to the fabrication of pyrolyzed transition metal macrocycles[2−5] and to the identification of the catalytic centers in the O_2 reduction mechanism.[6−11] M/N/C-based materials, synthesized by employing a multiplicity of metal, nitrogen, and carbon precursors, have been reported to exhibit promising electrocatalytic performance.[9,2,12−17] In particular, conjugated heterocyclic conducting polymers have been used as convenient nitrogen sources for the fabrication of M/N/C ORR electrocatalysts.[18,19,7,20−24] Among them, polypyrrole (PPy) is considered the most promising one[25] for the following reasons: (i) high electrical conductivity,[26] (ii) excellent support capability for catalysts such as metal oxides[27] and metal-based complexes,[28,29] and (iii) easy chemical[30] and electrochemical[31] synthesis routes. Currently, the most common methods to prepare Co/PPy electrocatalysts are (i) functionalization of carbon nanoparticles by chemical polymerization of pyrrole, followed by the chemical reduction or impregnation of a cobalt salt into the polymer;[22,32−34] (ii) fluidized-bed electropolymerization,[35] leading to the formation of a cobalt-modified PPy film supported on carbon nanoparticles; (iii) spraying or printing of carbon-supported Co/PPy incorporated into an ink; and (iv) direct electrodeposition using anodic polarization to electropolymerize pyrrole as a film and cathodic polarization to deposit the metal into the polymer structure.[36−39] However, the catalyst stability in acidic solution under oxygen reduction is the main problem hindering the practical replacement of the traditional Pt/C catalysts with M/N/C-based ones and has not yet been thoroughly investigated. Heat treatments have been found to be beneficial for electrodeposited polypyrrole−metal compounds, and in particular, both catalytic activity and durability have been found to increase drastically after pyrolysis,[22,37,40−45] the enhanced stability being attributed to the formation of active sites favoring the four-electron-transfer ORR pathway, thus reducing the peroxide generation rate.[46,47]

In the present paper we combine electrochemistry and quasi-in-situ X-ray photoelectron microspectroscopy to shed light on the morphology and composition of pyrolyzed Co/PPy

Received: June 25, 2014
Accepted: November 4, 2014
Published: November 4, 2014

 © 2014 American Chemical Society

electrocatalysts, whose precursors have been synthesized via the electrochemical route,[37−39] as well as on the changes occurring at different stages of aging under ORR conditions.

2. EXPERIMENTAL SECTION

2.1. Synthesis of Co/PPy Electrocatalyst. The Co/PPy electrocatalysts were fabricated following a two-step procedure: (i) electrochemical synthesis and (ii) pyrolysis.

The electrochemical synthesis of Co/PPy nanocomposites was performed using a classical three-electrode cell with a graphite disk (Φ = 10 mm) working electrode (WE), a Pt wire spiral (5 cm^2) counter electrode (CE), and an aqueous silver/silver chloride (Ag/AgCl/3 M: 0.209 V/NHE) reference electrode (RE), connected to the solution by a salt bridge. Coelectrodeposition was carried out in deaerated acetonitrile solutions containing 0.1 M pyrrole (Sigma-Aldrich, reagent grade, 98%), 0.05 M $CoCl_2{\cdot}6H_2O$ (Carlo Erba, 99%), 1% v/v H_2O, and 0.1 M TBAP (tetrabutylammonium perchlorate, Alfa Aesar, 99%) supporting electrolyte according to the step-pulsed potential procedure proposed in ref 37 and developed in our recent papers.[38,39] This particular pulse-plating process consists of the repetition of an optimized cycle consisting of (i) an initial step at 0 V for 1 s intended to relax the compositional double layer, (ii) a subsequent anodic pulse at +1.2 V for 0.5 s aimed at electrodepositing PPy, (iii) a cathodic step at −1.8 V for 0.5 s to incorporate the reduced Co species into PPy, and (iv) a final anodic step at +1.2 V for 0.2 s forming a capping layer of PPy. The potential values have been selected according to the cyclic voltammetric results reported in refs 37 and 39.

The pyrolysis of Co/PPy catalysts electrodeposited on graphite was realized in a tubular quartz flow reactor. N_2 at a flow rate of 80 cm^3 min^{-1} was used as the carrier gas. After purging with N_2 for 10 min, the temperature was increased at a rate of 10 °C min^{-1} up to 670 °C and then kept constant for 2 h.

2.2. ORR Aging Procedure. The aging of pyrolyzed Co/PPy electrodes was studied by recording successive ORR voltammograms in a stagnant O_2-saturated 0.5 M H_2SO_4 (Sigma-Aldrich 95−98%) electrolyte under quasi-steady-state conditions (5 mV s^{-1}). O_2 (SIAD: Società Italiana Acetilene e Derivati Spa) was allowed in the electrochemical chamber at 1 bar. The electrochemical measurements were performed at room temperature using a VersaStat potentiostat. In order to gain information on the stability of catalysts subjected to prolonged ORR, scanning photoelectron microscopy (SPEM) and micro-X-ray photoelectron spectroscopy (XPS) analyses have been conducted quasi-in-situ by applying three representative sets of aging conditions: 40, 140, and 300 voltammetric cycles.

2.3. FE-SEM. The morphology and quality of the Co/PPy catalysts electrodeposited on graphite disks and subsequently pyrolyzed were investigated by NVISION 40 Zeiss cross-beam focused ion beam (FIB) machine equipped with a high-resolution Gemini field emission gun (FEG) scanning electron microscope column, with a Ga source ion column and with an Oxford INCA 350 Xact energy dispersive X-ray spectrometer (EDX). Quantitative image analysis was performed with ImageJ software.

2.4. Scanning Photoelectron Microscopy (SPEM). SPEM measurements were carried out at the ESCA-microscopy beamline of the Elettra Synchrotron laboratory in Trieste,[48] operated in both photoelectron (PE) spectroscopy and imaging modes. PE spectra are measured from selected microspot regions, and PE maps are acquired by scanning the sample with respect to the microprobe, tuning the analyzer to the energy window of an element core level of interest. The present measurements were carried out with 1030 eV photon energy, 0.3 eV energy resolution, and 0.1 μm lateral resolution. More details about the SPEM setup and operation parameters can be found in refs 48−50.

The Co/PPy sample was mounted on a sample holder that bears an electrical connection allowing its use as a WE. Using an ultrahigh vacuum (UHV) compatible transfer arm, the electrode can be placed in contact with the electrolyte in a hanging-meniscus configuration in order to run the electrochemical reactions and, after the ORR treatment, can be transferred to the SPEM analysis station without exposure to air. The electrochemical cell, evacuated and keeping the electrolyte frozen using a liquid nitrogen trap, was filled with pure O_2 to atmospheric pressure, and then the electrolyte was warmed to room temperature (for details on our quasi-in-situ protocol, see ref 51). The aging of pyrolyzed Co/PPy electrodes was studied by recording successive ORR voltammograms in O_2-saturated 0.5 M H_2SO_4 aqueous electrolyte under quasi-steady-state conditions (5 mV s^{-1}) in a stagnant electrolyte.[52]

3. RESULTS AND DISCUSSION

3.1. FE-SEM and EDX Analyses. Figure 1 shows FE-SEM micrographs before and after pyrolysis of PPy (panels a and b)

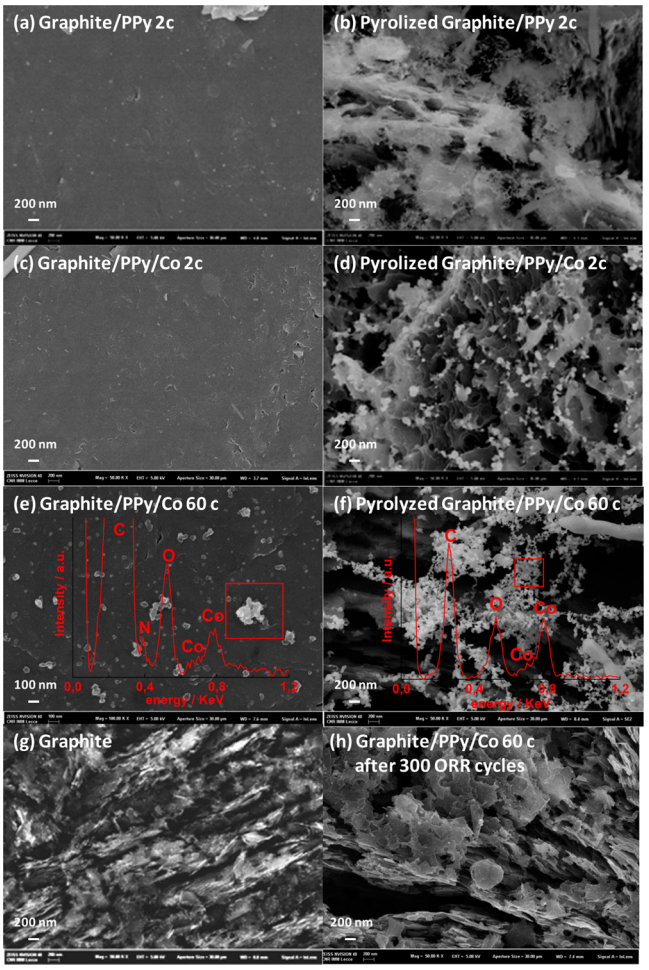

Figure 1. FE-SEM micrographs of PPy and Co/PPy electrodeposits (2 and 60 electrodeposition cycles) before (a, c, e) and after (b, d, f) pyrolysis. (g) Graphite electrode. (h) Co/PPy (60 electrodeposition cycles) after 300 cyclovoltammetric cycles of oxygen reduction aging (see Figure 2). The EDX spectra recorded for the areas within the red squares are overlapping the images in panels e and f.

and Co/PPy deposits after 2 (panels c and d) and 60 (panels e and f) pulse-plating cycles. The electropolymerization of polypyrrole leads in all cases to a film covering uniformly the graphite substrate (panels a, c, and e). Pyrolysis of the polymer gives rise to a mesh of uniformly distributed organic fragments (panel b), on which Co-containing nanoparticles can be clearly discerned when Co/PPy precursors are employed (panels d and f). By increasing the number of electrodeposition cycles from 2 (panel d) to 60 (panel f), progressive agglomeration of Co particles takes place (information regarding intermediate

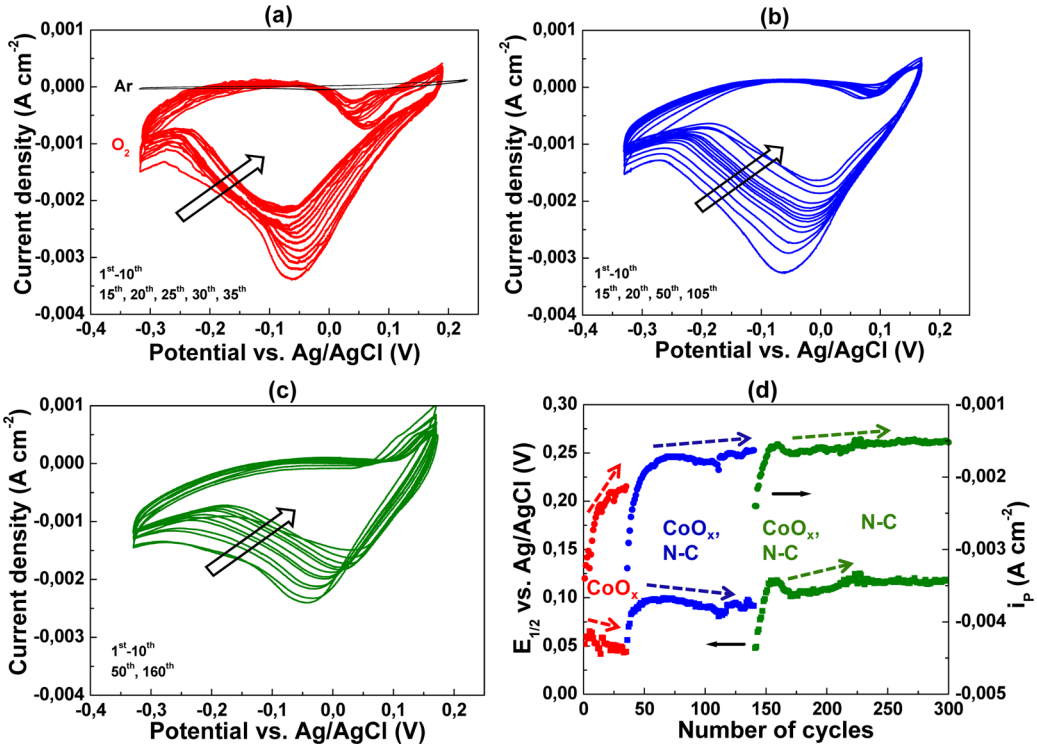

Figure 2. Quasi-steady-state cyclic voltammograms recorded in the electrochemical chamber connected to the SPEM analysis chamber. Electrode, Co/PPy (60 electrodeposition cycles); electrolyte, 0.5 M H_2SO_4 aqueous solution; scan rate, 5 mV s^{-1}; number of cycles, (a) 0−40, (b) 41−140, and (c) 141−300. (d) Variation of peak current density (i_p) and half-wave potential ($E_{1/2}$) with the number of cycles.

conditions, 20 and 40 cycles, is reported in Figure S1 of the Supporting Information).

The optimization of the pulse cycle number was performed on the basis of oxygen reduction electrocatalytic parameters (for quantitative details, see Table S1 in the Supporting Information) and identified 60 cycles as the best choice in view of electrocatalytic activity. The micrographs of the pyrolyzed sample after 60 electrodeposition cycles before ORR treatment (pristine) show a population of nanoparticles with a mean diameter of 19.6 nm and standard deviation of 9.6 nm. These particles are uniformly distributed over the main surface, as shown in the SEM images taken at lower magnifications (Figure S2a,b, Supporting Information) and resemble the typical morphology of calcined Co_3O_4 nanoparticles.[53] It is noteworthy that polypyrrole acts as a physical barrier to limit the sintering of particles during the thermal treatment.[54]

The presence of Co and oxygen in the particles was confirmed by the EDX spectra of as-electrodeposited (Figure 1e) and pyrolyzed (Figure 1f) Co/PPy, collected in different areas of 10 independently synthesized replicate samples. The nitrogen EDX peak (Figure 1e,f), clearly visible for unpyrolyzed Co/PPy, disappears after pyrolysis in agreement with XPS analysis (section 3.2.2). Panel h of Figure 1 reveals that Co grains of pyrolyzed Co/PPy (60 cycles of synthesis) tend to disappear after 300 ORR cycles, in agreement with SPEM results discussed in section 3.2.2. For comparison, in panel g we also report the morphology of the graphite support.

3.2. Co/PPy Aging Studied by Quasi-in-Situ Photoelectron Microspectroscopy. The surface morphochemical evolution of a typical pyrolized Co/PPy sample subjected to successive electrochemical aging treatments was studied by quasi-in-situ SPEM. The experimental procedure, detailed in the Supporting Information (Figure S3), involved sequential sample transfer between the O_2-pressurized electrochemical cell containing a 0.5 M H_2SO_4 aqueous solution, equipped with Pt QRE and CE, and the UHV SPEM analysis chamber. The SPEM setup has the capability of probing the same area after each electrochemical treatment, allowing single-grain spectroscopy.

3.2.1. ORR Cycling. The evolution of ORR electrocatalytic activity of the Co/PPy electrodes in the electrochemical chamber was monitored by measuring quasi-steady-state cyclic voltammograms. The same measurements, duplicated in argon atmosphere, indicate that the thermodynamically expected contribution of the Co(III)/Co(II) redox reaction is negligible with respect to the oxygen reduction current (black curve in Figure 2a and Figure S4 in the Supporting Information), in agreement with the literature regarding carbon-supported unpyrolyzed and pyrolyzed Co/PPy.[22,55] Possible explanations of the empirically assessed electrochemical stability are given in the Supporting Information.

Panels a−c in Figure 2 show the cyclovoltammetries corresponding to the three oxygen reduction aging steps we applied to the electrocatalyst—40, 140, and 300 cycles—whereas panel d shows the corresponding peak current densities (i_p) and the half-wave potential ($E_{1/2}$) variations. For each aging condition (0−40, 41−140, and 141−300 cycles), an initial transient followed by a stationary evolution of the considered parameter (i_p, $E_{1/2}$) can be observed. The i_p and the $E_{1/2}$ values gradually decrease inside the first and second aging stages, indicating a gradual decline in catalytic activity, similar to that observed for pyrolyzed cobalt macrocycles deposited by vacuum sublimation on a carbon support, where the decay of the active sites is attributed to the formation of highly oxidizing H_2O_2.[52] The damaging effect of H_2O_2—the reaction intermediate produced by the ORR two-electron

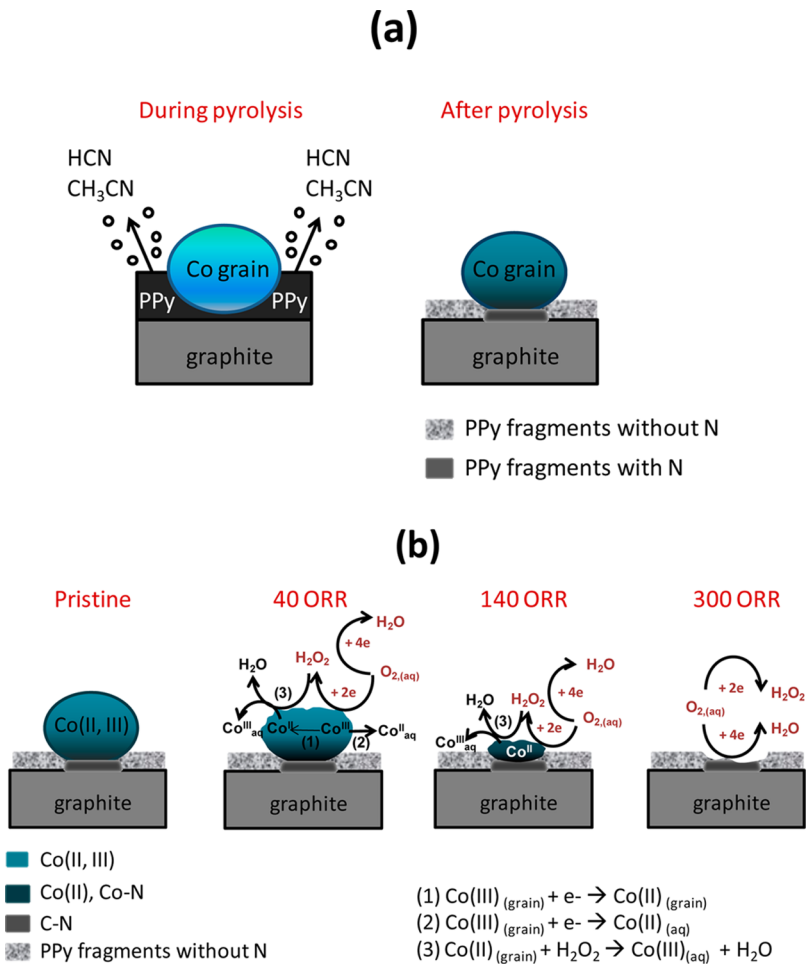

Figure 3. Schemes illustrating (a) the reason why N atoms are not revealed by XPS in the pristine pyrolyzed Co/PPy sample and (b) the morphochemical evolution of Co grains during oxygen reduction.

mechanism—toward Co grains during the oxygen reduction reaction takes place through the oxidation of Co(II) oxide to soluble Co(III) species according to eq 3 in Figure 3b. It is worth noting that the CoO/Co_3O_4 solid transition has been reported to be kinetically hindered in conditions similar to ours.[56]

In the third aging stage, the i_p value continues to decrease, while the $E_{1/2}$ value increases until a plateau is attained at ca. the 220th cycle. This behavior seems to denote a change in the ORR catalytic mechanism. The leaching of the Co particles pinpointed by SPEM (section 3.2.2) is in fact a factor liable to affect the catalyst activity.

3.2.2. SPEM Characterization of the Co/PPy Composites. The only elements that were observed in the XPS spectra of pristine samples were C, Co, and O. No detectable N 1s signal was measured in any location of the sample, in agreement with EDX results, while an intense N 1s pyrrolic-type signal typical of PPy materials[57] and unpyrolyzed Co/PPy[58] was measured before pyrolysis (Figure S5 of the Supporting Information). Positive evidence of PPy formation and measured N distributions before pyrolysis are also reported in a recent paper of ours.[39] The complexity of these findings confirms that N is lost during pyrolysis, according to the scheme of Figure 3a. At the temperature used in this work (670 °C), the polymer undergoes fragmentation and gasification, forming volatile species containing nitrogen, such as HCN or C_2H_3N.[59,60] During pyrolysis cobalt oxide, present on the surface of unpyrolyzed Co/PPy in the form of grains overhanging polypyrrole (Figure 1e), remains on the surface (Figure 1f), while the PPy layers lose N by gasification. This process is at least in part hindered under the cobalt grains, where active C−N and/or Co−N bonds can be formed (scheme of Figure 3a) and gradually appear with oxygen reduction aging (scheme of Figure 3b). The progressive vanishing of the N 1s XPS signal with increasing pyrolysis temperature is known in the case of Co/PPy supported on carbon particles.[61]

Figure 4a reports Co 2p, O 1s, and secondary electron background (BG) maps of a pristine pyrolyzed Co/PPy electrode. Since the sample is not perfectly flat, the contrast of the as-measured images contains significant contributions from surface topography that dominates the BG contrast. The grazing acceptance angle of the analyzer implemented at the ESCA microscopy beamline gives rise to the fact that electron emission is seemingly enhanced or attenuated by the topographic features;[49] nevertheless, despite these topography artifacts, one can clearly see the presence of distinct correlated bright regions in the Co and O maps. Such high local concentration of these elements is apparently due to the presence of Co oxide aggregates. This is confirmed by the micro-XPS spectra displayed in Figure 5. It is worth noting that, although the SPEM lateral resolution (~100 nm) is inferior to that of SEM, the SPEM maps reveal a morphology of the pristine sample that is very similar to that observed by SEM (Figure 1).

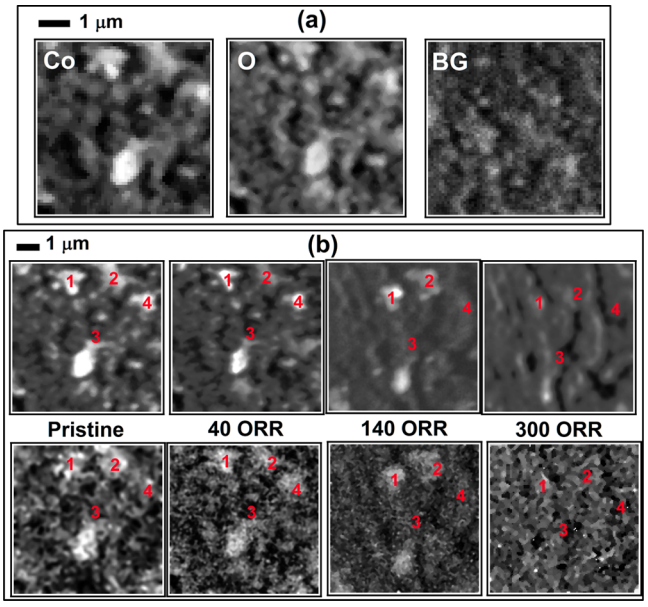

Figure 4. Quasi-in-situ SPEM maps of the same area of a pyrolyzed Co/PPy electrocatalyst. (a) Pristine conditions, with photoelectron micrographs measured at the Co 2p and O 1s energies and secondary electron background map (BG). (b) Photoelectron micrographs recorded at the Co 2p energy of the same region depicted in panel a under pristine and aged conditions (details reported on the image); upper row, raw maps; bottom row, minimized topography contribution (see the text). Aging was obtained by prolonged voltammetric cycling (see indications in the image and refer to Figure 2) in 0.5 M H_2SO_4 aqueous solution.

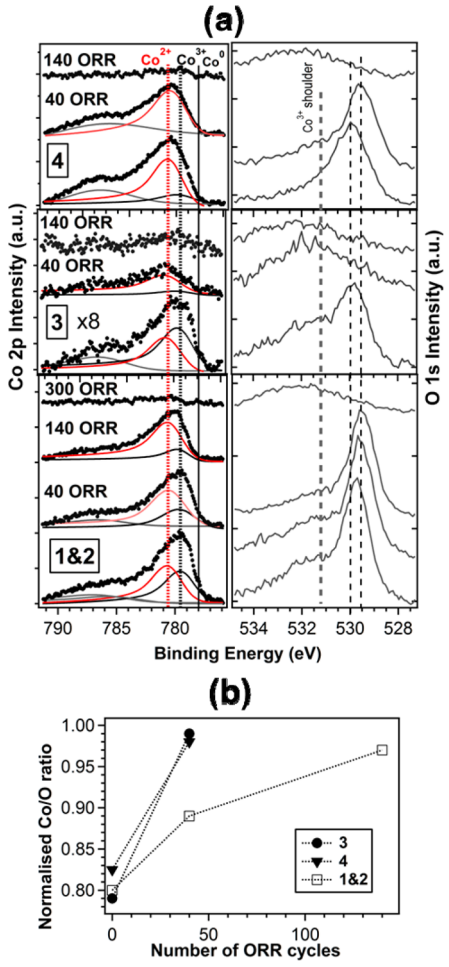

Figure 5. (a) Micro-XPS Co 2p and O 1s spectra measured at the points indicated in Figure 4 before and after various electrochemical aging steps. (b) Micro-XPS Co 2p/O 1s ratio as a function of the number of ORR voltammetric cycles.

The morphochemical evolution of the pristine sample, after successive application of 40, 140, and 300 ORR voltammetric cycles, was followed by both chemical imaging and micro-spectroscopic analysis. The upper row of Figure 4b shows the evolution of the Co 2p maps of a representative surface area. Using the image processing procedure developed in ref 62, which allows a strong reduction of the topographic contribution, we obtained the Co images displayed in the bottom row of Figure 4b, where the contrast is dominated exclusively by the distribution of the Co particles. The Co maps taken after successive ORR cycles clearly evidence that the amount of Co and the size of the Co aggregates gradually decrease and the bright areas, dominated by the Co signal, practically disappear after 300 ORR cycles.

Detailed chemical state information was obtained from the Co 2p and O 1s spectra, reported in Figure 5a, measured on the microspots denoted by the numbers 1−4 in the Co maps (Figure 4). The bottom spectrum in each subpanel corresponds to the initial (pristine) state. The selected areas represent four grains of the pristine sample with high (positions 1, 2, and 4) and low (position 3, ∼8 times less comparing the contrast and Co 2p signal) concentration of Co aggregates. The spectra taken in positions 1 and 2 under all the investigated conditions were practically identical, whereas the spectra measured in the other two areas show different initial chemical state and a different evolution during electrochemical aging. The correlative contrast of the Co 2p and O 1s maps clearly indicates that the chemical state of Co in the aggregates is that of an oxide. The two stable Co oxides are Co_3O_4 and CoO, which have characteristic Co 2p peaks at ∼779.5 and 780.2−780.6 eV, respectively, both shifted to higher binding energy with respect to the metallic Co peak at 778.3 eV.[63−66] The main Co(III) and Co(II) peaks also have satellites in the 786−789 eV energy range, the CoO one being significantly stronger.

Using this information we deconvoluted the measured Co 2p spectra using two components for the Co(III) and Co(II) peaks, respectively, and a single component for the satellite. The main O 1s peaks, corresponding to the two Co oxides, are positioned within the same energy range 529.5−530.0 eV, the Co_3O_4 having also a distinct shoulder at ∼531.2 eV. Peak deconvolution clearly reveals that in all regions both Co oxides are coexisting in the pristine state but with different ratios: Co_3O_4 dominates in the low Co concentration region 3, whereas CoO prevails in region 4.

As detailed above, the evolution of the chemical state in each location was followed after different degrees of aging by potential cycling in the ORR range. With an increasing number of ORR cycles, there is a clear trend of gradual reduction to CoO. This is accompanied by a decrease and disappearance of the Co 2p signal, in concert with the observed extinction of the Co oxide aggregates in the Co and O maps in Figure 4. The change in the Co oxidation state and the loss of the Co catalyst with aging is confirmed by the evolution of the corresponding O 1s spectra measured in locations 1−4. Since the O 1s spectra of the two Co oxides do not have very distinct differences, except for the shoulder at ∼531.2 eV for Co_3O_4, the line shape

change (loss of the shoulder and the small energy shift) can be attributed to an ongoing reduction process. The reduction of the Co_3O_4 to CoO with ORR cycles is also confirmed by the plots in panel b showing an increase of the Co 2p/O 1s ratio. However, the O 1s signal does not disappear completely like the Co 2p one: after the Co peak has faded away, a broad O 1s peak still remains, which is positioned at higher binding energy ~532 eV. The broad O 1s spectrum contains contributions from adsorbed O or O-containing species (e.g., OH, CO).[67−70] The increase in the CoO/Co_3O_4 ratio with the number of ORR cycles is the result of two main processes activated by aging: (i) the surface depletion of charge in the presence of acidic sites[71] (reaction 1, Figure 3) and (ii) the relative dissolution rates of Co(III) (reaction 2, Figure 3) and Co(II) oxides (reaction 3, Figure 3), operating on the initial Co(II) and Co(III) distribution within the pristine grain and resulting in a gradual change of the Co(II)/Co(III) at different stages of ORR cycling (scheme of Figure 3b).

These findings are in agreement with the cyclovoltammetric results shown in Figure 2d. The aging process leads to a monotonical decrease of the current density peak, in agreement with the progressive reduction of the area covered with Co aggregates and to the decrease and subsequent stabilization of the half-wave potential, correlated to the chemical nature of the catalyst. Undoubtedly, the decrease of the catalysts activity with cycling is a result not only of Co losses but also of complex modifications in the morphology and electronic structure of the surface, correlated with the particle size and Co chemical state.[71,72]

Close inspection of the XPS spectra revealed that the disappearance of Co oxide catalyst particles from the investigated locations is accompanied by the appearance and growth of the N 1s spectrum. Figure 6a shows that the N 1s signal emerges from the background after having applied 140 ORR cycles and that its intensity increases after 300. A similar trend was observed in all investigated locations. The N 1s spectra measured in the four locations of interest after 300 ORR cycles are displayed in Figure 6b. The line shapes of the N 1s spectra are clearly a result of several components and closely resemble those reported in the literature regarding pyrolyzed Co-PPy/carbon materials.[22,35,52,70,74,75] According to refs 70, 74, and 75, four different N-coordination types can be distinguished: (i) pyridinic N or (ii) metal-bonded N at 397−399.5 eV; (iii) pyrrolic N at 399.9−400.7 eV, and (iv) graphitic N at 401−403 eV. The N 1s spectrum shown in Figure 6b reveals the presence of pyridine-like and/or N−Co like (397 eV), pyrrolic (399.6 eV), and graphitic (400.6 eV) nitrogen in all the investigated areas. It is worth noting that in Co-deprived areas corresponding to the flat, C-rich background, the graphitic N component is more pronounced, indicating that N can also be bonded with carbon after pyrolysis. Thus, the residual catalytic activity found after the extinction of the Co 2p signal suggests that the removal of Co species from the surface can be the reason why the signal from C−N sites becomes detectable.

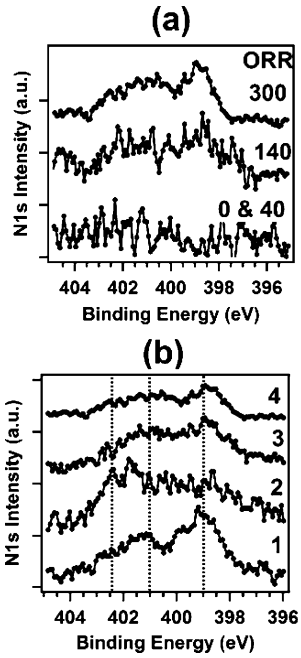

Figure 6. Micro-XPS N 1s spectra measured: (a) of point 4 at various aging stages and (b) after 300 ORR cycles of points 1−4. The point positions are indicated in Figure 4.

The initial high ORR activity of Co(II,III) oxides in the absence of N-sites (Figure 2a) indicates that cobalt plays a fundamental role on the ORR activity; moreover, the N−C moieties emerging since the second ORR stage (140 ORR) contribute to the ORR activity by stabilizing the half-wave potential decrease with aging.

4. CONCLUSIONS

The present study is focused on the electrochemical aging, under oxygen reduction reaction conditions, of pyrolized Co/PPy nanocomposites obtained by electrodeposition. Artificial aging of the electrocatalyts was achieved by subjecting the material, in contact with an acidic electrolyte, to a sequence of voltammetric cycles in the ORR potential range. Highly surface sensitive photoelectron microspectroscopy highlighted dramatic changes in surface composition, chemical state, and morphology that correlate with the decay of the electrocatalytic activity. The pristine electrocatalyst surface was found to consist of a mixture of Co(II) and Co(III) oxides in comparable amounts, aggregated in globular nanoparticles ~20 nm in diameter. Co 2p and O 1s spectra and chemical maps have revealed the gradual loss of Co from the surface, accompanied by partial reduction of the Co(III) oxide to the Co(II) form. The evolution of the amount of Co and of its chemical state correlate well with that of the cyclovoltammetric response. Moreover, after cobalt has practically vanished from the topmost surface layer as a result of prolonged cycling, the N 1s signal was found to appear and grow with aging: we have explained this behavior with the presence of C−N active sites in the deeper layers, correlating with the residual catalytic activity still measurable after the disappearance of cobalt from the surface.

In conclusion, the possibility of measuring quasi-in-situ and dynamically the compositional and chemical state space distribution of pristine and electrochemically aged Co/PPy with single-grain resolution has provided new and otherwise unattainable data for the molecular level understanding of some of the key factors determining the properties and durability of M/C/N-based ORR electrocatalysts.

■ ASSOCIATED CONTENT

Supporting Information

FE-SEM micrographs of pyrolyzed Co/PPy electrocatalyst after 20 and 40 electrodeposition cycles, FE-SEM micrographs of pyrolyzed Co/PPy electrocatalyst (60 electrodeposition cycles) at high magnifications, scheme of the procedure adopted for electrochemical quasi-in-situ SPEM measurements, ORR data for pyrolyzed Co/PPy electrodeposited at various pulse cycles, cyclic voltammetric analysis under Ar atmosphere of pyrolyzed Co/PPy (60 electrodeposition cycles) and pyrolyzed PPy electrode in the same conditions of ORR aging, micro-XPS N 1s spectrum for unpyrolyzed Co/PPy sample. This material is available free of charge via the Internet at http://pubs.acs.org.

■ AUTHOR INFORMATION

Corresponding Author

*E-mail: benedetto.bozzini@unisalento.it. Telephone: +39-0832-297323. Fax +39-0832-297733.

Author Contributions

The manuscript was written through contributions of all authors. All authors have given approval to the final version of the manuscript. All authors contributed equally.

Notes

The authors declare no competing financial interest.

■ ABBREVIATIONS USED

XPS = X-ray photoelectron spectroscopy
ORR = oxygen reduction reaction
SPEM = scanning photoelectron microscope

■ REFERENCES

(1) Jasinski, R. A New Fuel Cell Cathode Catalyst. *Nature* **1964**, *201*, 1212−1213.
(2) Gupta, S.; Tryk, D.; Bae, I.; Aldred, W.; Yeager, E. Heat-Treated Polyacrylonitrile-Based Catalysts for Oxygen Electroreduction. *J. Appl. Electrochem.* **1989**, *19*, 19−27.
(3) Gouérec, P.; Savy, M. Oxygen Reduction Electrocatalysis: Ageing of Pyrolyzed Cobalt Macrocycles Dispersed on an Active Carbon. *Electrochim. Acta* **1999**, *44*, 2653−2661.
(4) Bouwkamp-Wijnoltz, D. A. L.; Visscher, W.; Van Veen, J. A. R. The Selectivity of Oxygen Reduction by Pyrolysed Iron Porphyrin Supported on Carbon. *Electrochim. Acta* **1998**, *43*, 3141−3152.
(5) Gojković, S. L.; Gupta, S.; Savinell, R. F. Heat-Treated Iron(III) Tetramethoxyphenyl Porphyrin Chloride Supported on High-Area Carbon as an Electrocatalyst for Oxygen Reduction: Part III. Detection of Hydrogen-Peroxide during Oxygen Reduction. *Electrochim. Acta* **1999**, *45*, 889−897.
(6) Lalande, G.; Côté, R.; Guay, D.; Dodelet, J. P.; Weng, L. T.; Bertrand, P. Is Nitrogen Important in the Formulation of Fe-Based Catalysts for Oxygen Reduction in Solid Polymer Fuel Cells? *Electrochim. Acta* **1997**, *42*, 1379−1388.
(7) Chlistunoff, J. RRDE and Voltammetric Study of ORR on Pyrolyzed Fe/Polyaniline Catalyst. On the Origins of Variable Tafel Slopes. *J. Phys. Chem. C* **2011**, *115*, 6496−6507.
(8) Lefèvre, M.; Dodelet, J.-P.; Bertrand, P. Molecular Oxygen Reduction in PEM Fuel Cells: Evidence for the Simultaneous Presence of Two Active Sites in Fe-Based Catalysts. *J. Phys. Chem. B* **2002**, *106*, 8705−8713.
(9) C, M.; Proietti, E.; Jaouen, F. ; Dodelet, J. P. Iron-Based Catalysts with Improved Oxygen Reduction Activity in Polymer Electrolyte Fuel Cells. *Science* **2009**, *324*, 71−74.
(10) Charreteur, F.; Jaouen, F.; Ruggeri, S.; Dodelet, J.-P. Fe/N/C Non-Precious Catalysts for PEM Fuel Cells: Influence of the Structural Parameters of Pristine Commercial Carbon Blacks on their Activity for Oxygen Reduction. *Electrochim. Acta* **2008**, *53*, 2925−2938.
(11) Lee, D. H.; Lee, W. J.; Lee, W. J.; Kim, S. O.; Kim, Y.-H. Theory, Synthesis, and Oxygen Reduction Catalysis of Fe−Porphyrin-like Carbon Nanotube. *Phys. Rev. Lett.* **2011**, *106*, 175502−175505.
(12) Matter, P. H.; Zhang, L.; Otzkan, U. S. The Role of Nanostructure in Nitrogen-Containing Carbon Catalysts for the Oxygen Reduction Reaction. *J. Catal.* **2006**, *239*, 83−96.
(13) Matter, P. H.; Ozkan, U. S. Non-Metal Catalysts for Dioxygen Reduction in an Acidic Electrolyte. *Catal. Lett.* **2006**, *109*, 115−123.
(14) Matter, P. H.; Wang, E.; Millet, J. M. M.; Ozkan, U. S. Characterization of the Iron Phase in CNx-Based Oxygen Reduction Reaction Catalysts. *J. Phys. Chem. C* **2007**, *111*, 1444−1450.
(15) Sidik, R. A.; Anderson, A. B.; Subramanian, N. P.; Kumaraguru, S. P.; Popov, B. N. O_2 Reduction on Graphite and Nitrogen-Doped Graphite: Experiment and Theory. *J. Phys. Chem. C* **2006**, *110*, 1787−1793.
(16) Bezerra, C. W. B.; Zhang, L.; Lee, K. C.; Liu, H. S.; Zhang, J. L.; Shi, Z.; Marques, A. L. B.; Marques, E. P.; Wu, S. H.; Zhang, J. Novel Carbon-Supported Fe−N Electrocatalysts Synthesized through Heat Treatment of Iiron Tripyridyl Triazine Complexes for the PEM Fuel Cell Oxygen Reduction Reaction. *Electrochim. Acta* **2008**, *53*, 7703−7710.
(17) Kramm, U. I.; Herrmann-Geppert, I.; Bogdanoff, P.; Fiechter, S. Effect of an Ammonia Treatment on Structure, Composition, and Oxygen Reduction Reaction Activity of Fe−N−C Catalysts. *J. Phys. Chem. C* **2011**, *115*, 23417−23427.
(18) Peng, H.; Mo, Z.; Liao, S.; Liang, H.; Yang, L.; Luo, F.; Song, H.; Zhong, Y.; Zhang, B. High Performance Fe- and N-Doped Carbon Catalyst with Graphene Structure for Oxygen Reduction. *Sci. Rep.* **2013**, *3*, 1765.
(19) Wu, G.; L. More, K.; Johnston, C. M.; Zelenay, P. High-Performance Electrocatalysts for Oxygen Reduction Derived from Polyaniline, Iron, and Cobalt. *Science* **2011**, *332*, 443−447.
(20) Bashyam, R.; Zelenay, P. A Class of Non-Precious Metal Composite Catalysts for Fuel Cells. *Nature* **2006**, *443*, 63−66.
(21) Oh, H. S.; Oh, J. G.; Roh, B.; Hwang, I.; Kim, H. Development of Highly Active and Stable Non-Precious Oxygen Reduction Catalysts for PEM Fuel Cells Using Polypyrrole and a Chelating Agent. *Electrochem. Commun.* **2011**, *13*, 879−881.
(22) Lee, K. Z.; Lui, L.; Hui, H.; Shi, R.; Zhang, Z. J. Oxygen Reduction Reaction (ORR) Catalyzed by Carbon-Supported Cobalt Polypyrrole (Co-PPy/C) Electrocatalysts. *Electrochim. Acta* **2009**, *544*, 704−4710.
(23) Millan, W. M.; Thompson, T. T.; Arriaga, L. G.; Smit, M. A. Characterization of Composite Materials of Electroconductive Polymer and Cobalt as Electrocatalysts for the Oxygen Reduction Reaction. *Int. J. Hydrogen Energy* **2009**, *34*, 694−702.
(24) Liu, Y. C.; Hwang, B. J. Interaction of Copper(I)−Polypyrrole Complexes Prepared by Depositing−Dissolving Copper onto and from Polypyrroles. *Thin Solid Films* **1999**, *339*, 233−239.
(25) Yuan, X.; Ding, X.-L.; Wang, C.-Y.; Ma, Z.-F. Use of Polypyrrole in Catalysts for Low Temperature Fuel Cells. *Energy Environ. Sci.* **2013**, *6*, 1105−1124.
(26) Rasika Dias, H. V.; Fianchini, M.; Gamini Rajapakse, R. M. Greener Method for High-Quality Polypyrrole. *Polymer* **2006**, *47*, 7349−7354.
(27) Nguyen-Cong, H.; El-Abbassi, K.; Gautier, J. L.; Chartier, P. Oxygen Reduction on Oxide/Polypyrrole Composite Electrodes: Effect of Doping Anions. *Electrochim. Acta* **2005**, *50*, 1369−1376.
(28) Deronzier, A.; Moutet, J. C. Oxygen Reduction on Oxide/Polypyrrole Composite Electrodes: Effect of Doping Anions. *Coord. Chem. Rev.* **1996**, *147*, 339−371.
(29) Simon, E.; Sable, E.; Handel, H.; L'Her, M. Electrodes Modified by Conducting Polymers Bearing Redox Sites: Ni− and Co−Cyclam Complexes on Polypyrrole. *Electrochim. Acta* **1999**, *45*, 855−863.
(30) An, K. H.; Jeon, K. K.; Heo, J. K.; Lim, S. C.; Bae, D. J.; Lee, Y. H. High-Capacitance Supercapacitor Using a Nanocomposite Electrode of Single-Walled Carbon Nanotube and Polypyrrole. *J. Electrochem. Soc.* **2002**, *149*, A1058−A1062.

(31) Sadki, S.; Schottland, P.; Brodie, N.; Sabouraud, G. The Mechanisms of Pyrrole Electropolymerization. *Chem. Soc. Rev.* **2000**, *29*, 283−293.
(32) Olson, T. S.; Pylypenko, S.; Atanassov, P.; Asazawa, K.; Yamada, K.; Tanaka, H. Anion-Exchange Membrane Fuel Cells: Dual-Site Mechanism of Oxygen Reduction Reaction in Alkaline Media on Cobalt−Polypyrrole Electrocatalysts. *J. Phys. Chem. C* **2010**, *114*, 5049−5059.
(33) Yuan, X.; Zeng, X.; Zhang, H.-J.; Ma, Z.-F.; Wang, C.-Y. Improved Performance of Proton Exchange Membrane Fuel Cells with *p*-Toluenesulfonic Acid-Doped Co-PPy/C as Cathode Electrocatalyst. *J. Am. Chem. Soc.* **2010**, *132*, 1754−1755.
(34) Qin, H. Y.; Liu, Z. X.; Ye, L. Q.; Zhu, J. K.; Li, Z. P. The Use of Polypyrrole Modified Carbon-Supported Cobalt Hydroxide as Cathode and Anode Catalysts for the Direct Borohydride Fuel Cell. *J. Power Sources* **2009**, *192*, 385−390.
(35) Yuasa, M.; Yamaguchi, A.; Itsuki, H.; Tanaka, K.; Yamamoto, M.; Oyaizu, K. Modifying Carbon Particles with Polypyrrole for Adsorption of Cobalt Ions as Electrocatalytic Site for Oxygen Reduction. *Chem. Mater.* **2005**, *17*, 4278−4281.
(36) Ikeda, O.; Okabayashi, K.; Tamura, H. Electrocatalytic Reduction of Oxygen on Cobalt-Doped Polypyrrole Films. *Chem. Lett.* **1983**, *12*, 1821−1824.
(37) Masa, J.; Schilling, T.; Bron, M.; Schuhmann, W. Electrochemical Synthesis of Metal−Polypyrrole Composites and their Activation for Electrocatalytic Reduction of Oxygen by Thermal Treatment. *Electrochim. Acta* **2012**, *60*, 410−418.
(38) Bozzini, B.; Gianoncelli, A.; Bocchetta, P.; Dal Zilio, S.; Kourousias, G. Fabrication of a Sealed Electrochemical Microcell for in Situ Soft X-ray Microspectroscopy and Testing with in Situ Co−Polypyrrole Composite Electrodeposition for Pt-Free Oxygen Electrocatalysis. *Anal. Chem.* **2014**, *86*, 664−670.
(39) Bocchetta, P.; Gianoncelli, A.; Abyaneh, M. K.; Kiskinova, M.; Amati, M.; Gregoratti, L.; Jezeršek, D.; Mele, C.; Bozzini, B. Electrosynthesis of Co/PPy Nanocomposites for ORR Electrocatalysis: A Study Based on Quasi-in Situ X-ray Absorption, Fluorescence and in Situ Raman Spectroscopy. *Electrochim. Acta* **2014**, *137*, 535−545.
(40) Faubert, G.; Lalande, G.; Coté, R.; Guay, D.; Dodelet, J. P.; Weng, L. T.; Bertrand, P.; DeNes, G. Heat-Treated Iron and Cobalt Tetraphenylporphyrins Adsorbed on Carbon Black: Physical Characterization and Catalytic Properties of These Materials for the Reduction of Oxygen in Polymer Electrolyte Fuel Cells. *Electrochim. Acta* **1996**, *41*, 1689−1701.
(41) Yeager, E. Electrocatalysts for O_2 Reduction. *Electrochim. Acta* **1984**, *29*, 1527−1537.
(42) Wiesener, K. N_4-Chelates as Electrocatalyst for Cathodic Oxygen Reduction. *Electrochim. Acta* **1986**, *31*, 1073−1078.
(43) Ye, S.; Vijh, A. K. Cobalt-Carbonized Aerogel Nanocomposites Electrocatalysts for the Oxygen Reduction Reaction. *Int. J. Hydrogen Energy* **2005**, *30*, 1011−1015.
(44) Zhang, H. J.; Yuan, X.; Sun, L.; Zeng, X.; Jiang, Q. Z.; Shao, Z.; Ma, Z. F. Pyrolyzed CoN_4-chelate as an Electrocatalyst for Oxygen Reduction Reaction in Acid Media. *Int. J. Hydrogen Energy* **2010**, *35*, 2900−2903.
(45) Ji, Y.; Li, Z.; Wang, S.; Xu, G.; Yu, X. Thermal Treatment of Co(II) Tetracarboxyphenyl Porphyrin Supported on Carbon as an Electrocatalyst for Oxygen Reduction. *Int. J. Hydrogen Energy* **2010**, *35*, 8117−8121.
(46) Nallathambi, V.; Lee, J. W.; Kumaraguru, S. P.; Wu, G.; Popov, B. N. Development of High Performance Carbon Composite Catalyst for Oxygen Reduction Reaction in PEM Proton Exchange Membrane Fuel Cells. *J. Power Sources* **2008**, *183*, 34−42.
(47) Jaouen, F.; Dodelet, J.-P. O_2 Reduction Mechanism on Non-Noble Metal Catalysts for PEM Fuel Cells. Part I: Experimental Rates of O_2 Electroreduction, H_2O_2 Electroreduction, and H_2O_2 Disproportionation. *J. Phys. Chem. C* **2009**, *113*, 15422−15432.
(48) Abyaneh, M. K.; Gregoratti, L.; Amati, M.; Dalmiglio, M.; Kiskinova, M. Scanning Photoelectron Microscopy: A Powerful Technique for Probing Micro and Nano-Structures. *e-J. Surf. Sci. Nanotechnol.* **2011**, *9*, 158−162.
(49) Gregoratti, L.; Marsi, M.; Cautero, G.; Kiskinova, M.; Morrison, G. R.; Potts, A. W. Spectromicroscopy of Interfaces with Synchrotron Radiation: Multichannel Data Acquisition. *Nucl. Instrum. Methods Phys. Res., Sect. A* **2001**, *467*, 884−888.
(50) Günther, S.; Kaulich, B.; Gregoratti, L.; Kiskinova, M. Photoelectron Microscopy and Applications in Surface and Material Science. *Prog. Surf. Sci.* **2002**, *70*, 187−260.
(51) Bozzini, B.; Amati, M.; Abyaneh, M. K.; Gregoratti, L.; Kiskinova, M. An Investigation into the Initial Stages of the Electrochemical Reduction of Cr(VI) at Pt(111), Based on Scanning Photoelectron Microscopy. *J. Electroanal. Chem.* **2011**, *657*, 113−116.
(52) Feng, J.; Liang, Y.; Wang, H.; Li, Y.; Zhang, B.; Zhou, J.; Wang, J.; Regier, T.; Dai, H. Engineering Manganese Oxide/Nanocarbon Hybrid Materials for Oxygen Reduction Electrocatalysis. *Nano Res.* **2012**, *5*, 718−725.
(53) Qingwen, L.; Guoan, L.; Youqin, S. Response of Nanosized Cobalt Oxide Electrodes as pH Sensors. *Anal. Chim. Acta* **2000**, *409*, 137−142.
(54) Cho, Y.; Lee, W. H.; Kim, H. A Novel Synthetic Route for the Preparation of Core Shell Like Carbon-Supported Nanoparticles with a Pt-Rich Shell. *J. Mater. Chem. A* **2014**, *2*, 11635−11641.
(55) Feng, W.; Li, H.; Cheng, X.; Jao, T.-C.; Weng, F.-B.; Su, A.; Chiang, Y.-C. A Comparative Study of Pyrolyzed and Doped Cobalt-Polypyrrole Eletrocatalysts for Oxygen Reduction Reaction. *Appl. Surf. Sci.* **2012**, *258*, 4048−4053.
(56) Kozhina, G. A.; Ermakov, A. N.; Fetisov, V. B.; Fetisov, A. V.; Shunyaev, K. Yu. Electrochemical Dissolution of Co_3O_4 in Acidic Solutions. *Russ. J. Electrochem.* **2009**, *45*, 1170−1175.
(57) Atanasoska, L.; Naoit, K.; Smyrl, W. H. XPS Studies on Conducting Polymers: Polypyrrole Films Doped with Perchlorate and Polymeric Anions. *Chem. Mater.* **1992**, *4*, 988−994.
(58) Lee, K.; Zhang, L.; Lui, H.; Hui, R.; Shi, Z.; Zhang, J. Oxygen Reduction Reaction (ORR) Catalyzed by Carbon-sSupported Cobalt Polypyrrole (Co-PPy/C) Electrocatalysts. *Electrochim. Acta* **2009**, *54*, 4704−4711.
(59) Uyar, T.; Toppare, L.; Hacaloğlu, J. Characterization of Electrochemically Synthesized *p*-Toluene Sulfonic Acid Doped Polypyrrole by Direct Insertion Probe Pyrolysis Mass Spectrometry. *J. Anal. Appl. Pyrolysis* **2002**, *64*, 1−13.
(60) Hong, X.; Zhang, L.; Zhang, T.; Qi, F. An Experimental and Theoretical Study of Pyrrole Pyrolysis with Tunable Synchrotron VUV Photoionization and Molecular-Beam Mass Spectrometry. *J. Phys. Chem. A* **2009**, *113*, 5397−5405.
(61) Qin, H.; Lao, S.; Liu, Z.; Zhu, J.; Li, Z. Effects of Heat Treatment on the Structure, Morphology and Electrocatalytic Activity of Cobalt Hydroxide Electrocatalyst. *Int. J. Hydrogen Energy* **2010**, *35*, 1872−1878.
(62) Gregoratti, L.; Barinov, A.; Benfatto, E.; Cautero, G.; Fava, C.; Lacovig, P.; Lonza, D.; Kiskinova, M.; Tommasini, R.; Mähl, S.; Heichler, W. 48-Channel Electron Detector for Photoemission Spectroscopy and Microscopy. *Rev. Sci. Instrum.* **2004**, *75*, 64−68.
(63) Yang, W.-H.; Kim, M. H.; Ham, S.-W. Effect of Calcination Temperature on the Low-Temperature Oxidation of CO over CoO_x/TiO_2 Catalysts. *Catal. Today* **2007**, *123*, 94−103.
(64) Petitto, S. C.; Marsh, E. M.; Carson, G. A.; Langell, M. A. Cobalt Oxide Surface Chemistry: The interaction of CoO(1 0 0), Co_3O_4(1 1 0) and Co_3O_4(1 1 1) with Oxygen and Water. *J. Mol. Catal. A: Chem.* **2008**, *281*, 49−58.
(65) Zafeiratos, S.; Dintzer, T.; Teschner, D.; Blume, R.; Hävecker, M.; Knop-Gericke, A.; Schlögl, R. Methanol Oxidation over Model Cobalt Catalysts: Influence of the Cobalt Oxidation State on the Reactivity. *J. Catal.* **2010**, *269*, 309−317.
(66) Biesinger, M. C.; Payne, B. P.; Grosvenor, A. P.; Lau, L. W.M.; Gerson, A. R.; St. C. Smart, R. Resolving Surface Chemical States in XPS Analysis of First Row Transition Metals, Oxides and Hydroxides: Cr, Mn, Fe, Co and Ni. *Appl. Surf. Sci.* **2011**, *257*, 2717−2730.

(67) Oku, M.; Hirokawa, K.; Ikeda, S. X-ray Photoelectron Spectroscopy of Manganese−Oxygen Systems. *J. Electron Spectrosc.* **1975**, *7*, 465−473.
(68) Barr, T. L.; Fries, C. G.; Cariati, F.; Bart, J. C.; Giordano, N. A Spectroscopic Investigation of Cerium Molybdenum Oxides. *J. Chem. Soc., Dalton Trans.* **1983**, 1825−1829.
(69) Larachi, F.; Pierre, J.; Adnot, A.; Bernis, A. Ce 3d XPS Study of Composite $Ce_xMn_{1-x}O_{2-y}$ Wet Oxidation Catalysts. *Appl. Surf. Sci.* **2002**, *195*, 236−250.
(70) Zhang, H. J.; Kong, H. C.; Yuan, X. X.; Jiang, Q. Z.; Yang, J. H.; Ma, Z. F. Influence of Metal Precursors on the Catalytic Activity and Structure of Non-Precious Metal Electrocatalysts for Oxygen Reduction Reaction. *Int. J. Hydrogen Energy* **2012**, *37*, 13219−13226.
(71) Martin-González, M. S.; García, M. A.; Lorite, I.; Costa-Krämer, J. L.; Rubio-Marcos, F.; Carmona, N.; Fernández, J. F. A Solid-State Electrochemical Reaction as the Origin of Magnetism at Oxide Nanoparticle Interfaces. *J. Electrochem. Soc.* **2010**, *157*, E31−E35.
(72) Bozzini, B.; Amati, M.; Boniardi, M.; Kazemian Abyaneh, M.; Gregoratti, L.; Kiskinova, M. Study of a Proton Exchange Membrane Fuel Cells Catalyst Subjected to Anodic Operating Conditions, by Synchrotron-based Scanning Photoelectron Microscopy (SPEM) and High Lateral-Resolution X-ray Photoelectron Spectroscopy. *J. Power Sources* **2011**, *196*, 2513−2518.
(73) Mayrhofer, K. J. J.; Blizanac, B. B.; Arenz, M.; Stamenkovic, V. R.; Ross, P. N.; Markovic, N. M. The Impact of Geometric and Surface Electronic Properties of Pt-Catalysts on the Particle Size Effect in Electrocatalysis. *J. Phys. Chem. B* **2005**, *109*, 14433−14440.
(74) Roe, S. P.; Hill, J. O.; Magee, R. J. Spectroscopic Studies on Some Pyridine and Morpholine Adducts of (meso-Tetraphenylporphyrin)chromium(III) Chloride. *Aust. J. Chem.* **1986**, *39*, 1377−1383.
(75) Pylypenko, S.; Mukherjee, S.; Olson, T. S.; Atanassov, P. Non-Platinum Oxygen Reduction Electrocatalysts based on Pyrolyzed Transition Metal Macrocycles. *Electrochim. Acta* **2008**, *53*, 7875−7883.